15 High Power Quantum Dot Lasers

Christian Ribbat and Roman Sellin

15.1 High Power Laser Diodes

Motivation for and applications of high power diode lasers are briefly summarized, followed by a short description of the main technological approaches to meet the desired application criteria. In 15.2 the quantum dot (QD) growth in respect to laser applications and the heterostructure QD laser design are discussed and key results of high power QD lasers are presented.

15.1.1 Applications of High Power Laser Diodes

High power diode lasers are commonly used as pump sources for either fiber amplifiers like EDFAs (erbium doped fiber amplifiers) or for solid state lasers like Nd:YAG-lasers. However, the economically most relevant application of high power lasers is in telecommunication. Diode lasers at 980 nm are commonly used as optical pump sources for erbium doped fiber amplifiers for long distance optical fiber communication at 1.55 µm. In recent years diode lasers also found applications in direct material processing like welding or metal hardening (carburisation) [1]. Advantages are high efficiency, high optical output power, compactness and modularity of these systems. With the concept of laser bars high optical output powers of several hundred Watt up to kW were demonstrated in continuous-wave operation [2–5]. Due to high wall-plug efficiencies (50%-60%) cooling systems can be kept small. Thus compact modules can be realized. A relevant future application might also be the optical pumping of other fiber amplifiers, like thulium or erbium doped fluoride fiber lasers which emit in the green and blue spectral range [6]. As thulium can be pumped very efficiently at 1120 nm, such a system would be very interesting for future laser display technologies. Nevertheless high power laser diodes beyond 1100 nm, based on standard InGaAs/GaAs quantum well technology, are presently commercially not available.

15.1.2 Requirements for High Power Laser Diodes

High power laser diodes are operated at very high injection currents to reach the required high output powers. To manage the high thermal load generated by high electric and optic power densities within the laser device, good

M. Grundmann (ed.), *Nano-Optoelectronics*
© Springer-Verlag Berlin Heidelberg 2002

thermal stability of threshold current and quantum efficiency is required. A corresponding problem due to the very high optical power density at the front facet is facet degradation. Especially catastrophic optical mirror damage (COD) results in sudden failure of the device. As most applications demand coupling of the emitted radiation into optical fibers, sophisticated approaches are used to increase coupling efficiency, e.g. the use of large optical cavity (LOC) wave-guide structures for optimized far field distribution.

High wall-plug efficiency is needed to avoid that the output power of a laser diode is limited by thermal roll-over. This is realized by high internal quantum efficiency, low internal optical loss and an optimized current-voltage characteristic. One way to improve the latter is to use long cavities to reduce the ohmic resistivity (L=1.0–4.0 mm). Therefore low internal optical losses, typically around 1 cm^{-1}, have to be reached not to jeopardize the optical output power. Furthermore, a good mounting technique for excess heat reduction and a high thermal stability of the laser performance are also required to avoid thermal roll over and guarantee long term stability. To delay the onset of COD, sophisticated techniques of facet coatings are applied [1]. Dielectric mirror coatings are deposited on the laser facets to passivate and protect the extremely sensitive surface and to change the reflectivity (R) such the total optical output power is emitted from the front facet. Typically high reflection coatings of $R \simeq 90\%$ reflectivity are applied at the back facet, using $\lambda/4$-pairs of Si/Al_2O_3 or SiO_2/SiN_x. A low reflection coating of R =3%–20% is used for the front facet.

High brightness of the laser radiation is demanded for most applications, especially with respect to coupling into fiber optics. For these applications the optical power within the fiber rather than the total output power is of interest. To improve the coupling efficiency of laser diodes into fiber optics, especially in single mode fibers, filamentation of the lasing mode has to be suppressed even at very high output powers. Lateral ground mode lasing is realized in small stripe-width lasers, typically 4–6 µm. Also shallow mesa structures where the optical mode is only weakly index guided are applied. However, as a small stripe width reduces the possible maximum output power due to the onset of COD, tapered structures have been developed to realize broad-area lasing with suppressed filamentation. To reduce the beam divergence in the fast axis (vertical direction) large optical cavity (LOC) structures are applied. To suppress the onset of higher order transverse modes the cladding layers have to be designed appropriately [7].

15.1.3 Advantages of Quantum Dot Lasers for High Power Applications

Today quantum dot lasers demonstrate the lowest threshold current densities of any semiconductor laser. The improvement of the threshold current for bulk, quantum well and quantum dot lasers can be seen in Fig. 1.4. This is due to the reduced density of states for QD lasers as compared to bulk or QW

lasers. Especially for long cavity devices that operate close to transparency the reduced number of states that have to be inverted to reach lasing favors the QD approach. A low threshold current is also favorable for high power operation as it reduces the heat generation within the device.

Based on theoretical considerations QD lasers were supposed to be temperature insensitive with respect to threshold current [8]. As mentioned, this would be very beneficial for high power operation. However, as discussed in Sect. 12.5, this prediction does not hold true in the case of multi-level QDs with finite barrier heights.

One other advantage of QD as compared to QW lasers is the decreased in-plane carrier diffusion due to the localization of the carriers in the QDs [9–11]. Reduction of the mirror degradation and reduced filamentation in broad-area lasers [12] are therefore predicted. As the latter is also strongly dependent on the linewidth enhancement factor (α-factor) [13,14], QD lasers with strongly reduced α-factor [12] are also supposed to demonstrate improved filamentation stability as compared to QW lasers.

Finally one of the major advantages of the QD concept is the tunability of the emission wavelength by QD size and composition. Additionally this technique offers the extension of the possible wavelength regime further into the infrared on GaAs substrates. Due to this possibility totally new applications for high power diode lasers emerge like e.g. the thulium doped fluoride-fiber amplifier for blue lasing or telecom pump-lasers at 1.48 µm based on GaAs technology.

15.2 Quantum Dot Lasers

15.2.1 MBE and MOCVD Growth

The concepts and fundamentals of QD growth have already been described in chapter [Madhukar]. Here only some issues concerning particularly high power laser applications will be addressed. A key parameter for a laser device is the modal gain of the active region. In order to reach ground-state lasing a sufficiently high QD density with a small size distribution of the QDs has to be achieved. If the QD density of one layer is not high enough for the modal gain to surpass the internal optical and mirror losses, several sheets of QDs might be stacked and incorporated into the wave-guide region. Typically one up to ten sheets of QDs are used for QD lasers with a dot density of $2 \times 10^{10}\,\mathrm{cm}^{-2}$ to $1 \times 10^{11}\,\mathrm{cm}^{-2}$ and an inhomogeneous broadening of 50–100 meV. We note that high densities of small InGaAs/GaAs QDs, typically emitting below 1.1 µm can be easily achieved. However, for larger QDs, e.g. for 1.3 µm emission, sophisticated techniques such as the seeding concept or spinodal decomposition [15] have to be applied to ensure a sufficiently large density of large QDs (see Sect. 13.3). Apart from ensuring a sufficiently high QD density with small inhomogeneous broadening, the challenge of QD laser device growth lies in the defect-reduction of the QDs and the barrier

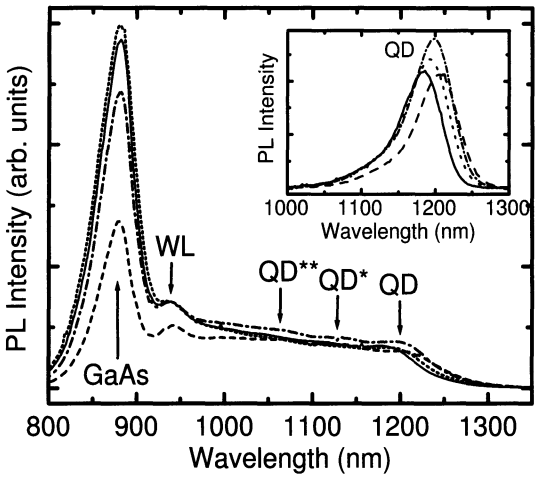

Fig. 15.1. PL spectra for high excitation density (5 kWcm^{-2}) and for low excitation density (5 Wcm^{-2}, inset), recorded at room temperature for samples with different annealing times t_A (no annealing: *dashed line*, 10 min: *solid line*, 20 min: *dotted line*, and 30 min: *dash-dotted line*). Arrows indicate the positions of the QD ground state (QD) and excited state transitions (QD*, QD**), the wetting layer (WL) and the GaAs matrix material. The different samples contain QDs annealed at 600°C for the denoted annealing durations

materials. Furthermore a flat growth front is desired. An in-situ annealing process was developed to improve the GaAs matrix quality which will be described here shortly:

The QDs are grown at 490°C and than capped with a 7 nm thick GaAs layer. During the growth of this layer the temperature is ramped from 490°C up to 600°C. For several minutes a growth interruption is applied under AsH_3 stabilized conditions. Figure 15.1 shows photoluminescence (PL) spectra of test structures for four different annealing times ($t_A = 0, 10, 20$ and 30 min) recorded at high excitation density. The intensity from the GaAs matrix increases by a factor of about two upon annealing for 10 or 20 min. The

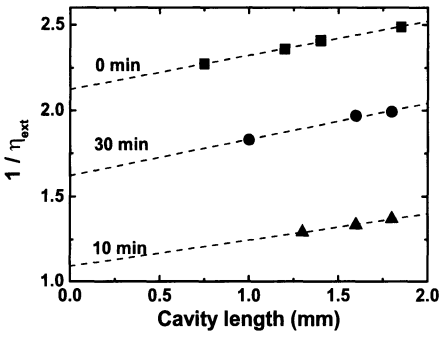

Fig. 15.2. Inverse external quantum efficiency η_{ext}^{-1} as a function of cavity length for different annealing durations with linear fits (*dashed lines*). Stripe widths are 75 µm. An estimated error of about 10% can be assumed

saturated PL intensity from the QDs remains essentially unchanged with respect to its spectral position and intensity for all growth interruptions. The QDs are practically not altered by the annealing step. This is also visualized in the spectra recorded at low excitation density (see inset of Fig. 15.1) when the QD ground state is not saturated. The increase of the GaAs luminescence might be explained by a reduction of two different kinds of defects that are both related to the growth of the quantum dot layers.

First, misfit dislocations might be formed on a very small fraction of the QDs, most likely by very large ones. These dislocations proceed into the GaAs on top of them and strongly reduce the GaAs luminescence, acting as non-radiative recombination centers. An in-situ annealing step with the surface being very close to the spatial origin of the dislocations enables strong reduction of the number of dislocations, as demonstrated in [16] by deep level transient spectroscopy (DLTS). However, as the number of dislocation-containing or -inducing QDs is small as compared to the number of QDs in which recombination occurs radiatively, no significant improvement of the QD luminescence itself is observed upon annealing. Thus we assume the QDs to be of high crystalline quality even without annealing. Secondly, point defects in the first 2–3 nm of the low-temperature GaAs grown at 490°C immediately on top of the QDs may act as non-radiative recombination centers. Typical MOCVD growth temperatures for low defect density bulk GaAs are in the range of 600°C to 650°C. GaAs grown at lower temperatures tends to build non-equilibrium point defects.

Figure 15.2 depicts η_{ext}^{-1} as a function of the cavity length for $t_{\text{A}} = 0, 10,$ and 30 min. We obtain internal quantum efficiencies of η_{int} =47% (0 min), $\eta_{\text{int}} = 92\%$ (10 min), and $\eta_{\text{int}} = 62\%$ (30 min), in correlation with the GaAs matrix quantum efficiency (Fig. 15.1) (with an estimated error of 10%). η_{int} is thus strongly enhanced up to a value above 90% for $t_{\text{A}} = 10$ min. The improvement of the differential internal quantum efficiency is due to the improvement of the barrier material and the reduction of related leakage currents. The internal losses derived from the slope of the fits are $2.1 \pm 0.5\,\text{cm}^{-1}$ (0 min), $1.5 \pm 0.3\,\text{cm}^{-1}$ (10 min), and $2.10 \pm 0.04\,\text{cm}^{-1}$ (30 min). The reduction of the internal loss with annealing time can be attributed to a smoothing of the upper wave-guide interface. This is confirmed by an atomic force microscopy (AFM) study of the growth front showing a strong reduction of surface roughness upon the annealing step. More details of this process can be found in [17,18].

15.3 Characteristics of Ridge Wave-Guide Quantum Dot Lasers

Figure 15.3 presents a schematic layout of a laser with three sheets of QDs. Fig. 15.3b shows a cross-section transmission electron microscopy (TEM) image of the active region with three sheets of QD layers and the inset below

Fig. 15.3c presents a plan-view TEM-image of a QD layer (taken under dark-field conditions). Like in conventional high power diode lasers AlGaAs or InGaP cladding layers, GaAs wave-guide and shallow mesa stripes have been used for the ridge wave-guide lasers.

One limiting factor of maximum output power is the COD level. In order to rule out oxidation of the AlGaAs cladding layers one can choose an Al-free design using indium-gallium-phosphide (InGaP) as cladding material. So far the highest COD-level for a QD laser of 20 $MWcm^{-2}$ for uncoated facets has been achieved with this approach [19,20]. In principle all measures to suppress the onset of COD in QW-based lasers can be applied to QD lasers, too. These are primarily sophisticated passivation and coatings of the laser facets or the employment of large optical cavities to reduce the optical power density at the front facet.

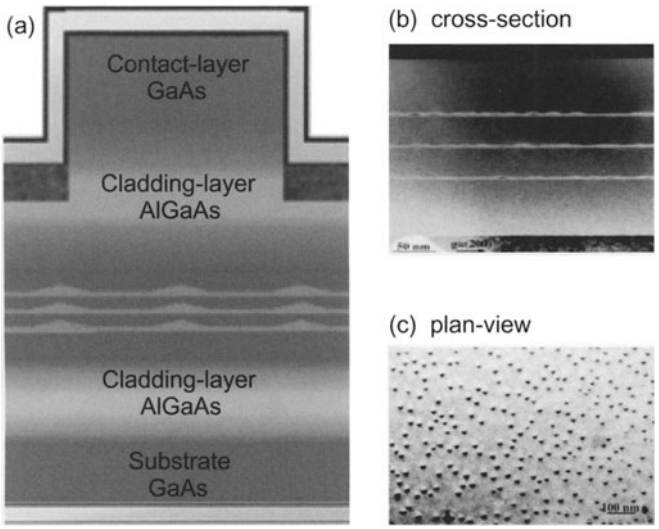

Fig. 15.3. Schematic wave-guide structure of a QD laser, (**a**) heterostructure of an AlGaAs QD laser, 30%–60% AlGaAs cladding layers with 0.2–0.8 µm GaAs wave-guide, (**b**) cross-section transmission electron microscopy (TEM) image of the active zone (three-fold QD stacks), (**c**) plan-view high resolution TEM image of the QD sheet (dot density $5 \times 10^{10} cm^{-2}$). TEM images performed at the Max-Planck-Institute für Mikrostrukturphysik in Halle, Germany

15.3.1 Output Power

Early theoretical calculations predicted a phonon bottleneck for QDs. Retarded carrier due to the phonon bottleneck degrade threshold current and external quantum efficiency [21,22]. However, QD lasers could demonstrate

high optical output powers with high quantum efficiency and low threshold current densities [17,19,23–28]. As described in chapter [by Robert] the phonon bottleneck holds only true for isolated QDs. If the QDs are surrounded by carriers there exist various processes that circumvent this limitation. Experimental studies show refilling times of QDs as fast as 65 ps [29].

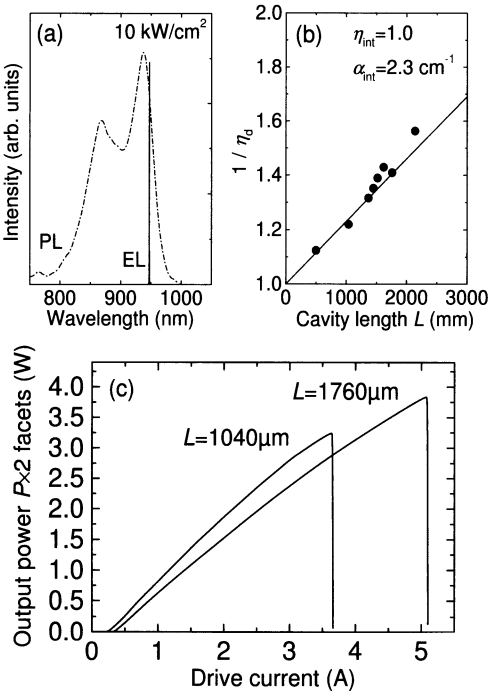

Fig. 15.4. Light-output characteristics of MBE-grown broad-area QD lasers (after [30]), (**a**) high excitation (room temperature) photoluminescence spectra and lasing line of QD laser, (**b**) reciprocal external differential quantum efficiency versus cavity length (the linear fit yields an internal quantum efficiency close to 100% and an optical loss $\alpha_{\text{int}} = 2.3\,\text{cm}^{-1}$) and (**c**) output power versus drive current for 100 µm broad-area QD laser at 940 nm. The cavity lengths are 1.05 mm and 1.76 mm, threshold current densities 316 Acm^{-2}, 188 Acm^{-2}, slope efficiencies 82%, 70% and the maximum optical output power are 3 W and 4 W, respectively

Figure 15.4 presents the characteristics of a 940 nm MBE-grown QD laser [30]. Figure 15.4a depicts the photoluminescence spectra of the ground state and the first excited state as well as the electroluminescence lasing line. Fig. 15.4b shows the reciprocal external quantum efficiency versus the cavity length. From the linear fit an internal differential quantum efficiency close to 100% and an internal optical loss of 2.3 cm^{-1} are deduced. A total optical output power close to 4 W in cw operation is demonstrated for a 1.76 mm long device with 100 µm stripe width, a threshold current density of 188 Acm^{-2} and 70% differential quantum efficiency. A shorter device with 1.04 mm cavity length demonstrates more than 3 W optical output power with 82% external quantum efficiency and a threshold current density of 316 Acm^{-2}. In these cases, the output power of the lasers with as-cleaved facets was limited by COD.

This is in close agreement to results reported in [28] were 4 W cw output power, 90% internal quantum efficiency and a total wall-plug efficiency > 50% at 980 nm were demonstrated for MBE-grown QD lasers.

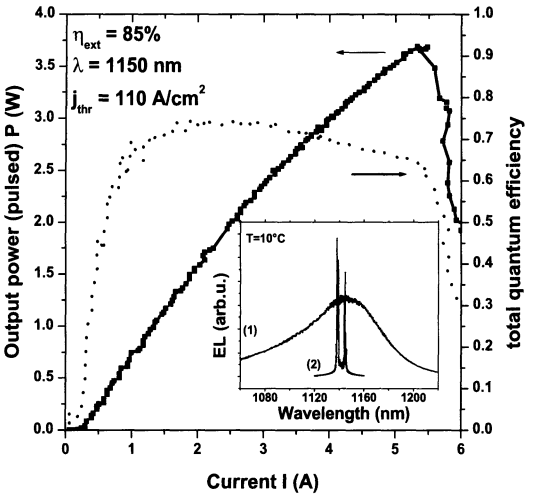

Fig. 15.5. Light-output characteristics of MOCVD-grown broad-area QD lasers (pulsed mode, f=1 kHz, pulse-width 0.8 µs, as-cleaved facets, mounted p-side up, 200 µm stripe-width, 1.3 mm cavity length): 4 W maximum power at 1150 nm, 85% external quantum efficiency, 110 Acm^{-2} threshold current density. The inset shows electroluminesence spectra below and shortly above threshold

In Fig. 15.5 the output characteristics for a MOCVD-grown QD laser emitting at 1150 nm is presented. With a stripe width of 200 µm (mounted p-side up and as-cleaved facets) this laser demonstrates a maximum optical output power close to 4 W in pulsed operation. The external quantum efficiency has been as high as 85% and the threshold current density was 110 Acm^{-2} [25]. The electroluminescence spectra below threshold (spontaneous emission) (1) and shortly above threshold (stimulated emission) (2) are shown in the inset. The linear fit of the reciprocal external quantum efficiency as a function of cavity length yields an internal quantum efficiency close to 100% and an internal optical loss of 1.5 cm^{-1}.

Thus for both epitaxial growth techniques, MBE and MOCVD, a high internal quantum efficiencies close to ideal 100% could be demonstrated accompanied by internal losses of $\alpha_{\text{int}} = 2.3\,\text{cm}^{-1}$ (MBE) and $\alpha_{\text{int}} = 1.5\,\text{cm}^{-1}$ (MOCVD), sufficient for high power applications.

15.3.2 Threshold Current Density

One of the early predicted advantages of QD lasers as compared to QW lasers is low threshold current density [31] which today has been demonstrated in numerous experiments [32–34]. The transparency current densities, $j_{\text{thr}}(L \to \infty)$, for InGaAs single QW lasers is typically about 50 Acm^{-2}. For single-sheet QD lasers at 1.26 µm, extremely low threshold current densities of 16 Acm^{-2} [34] could be demonstrated. Even though high power lasers are operated well above threshold, a reduced threshold current is still favorable as it decreases excess heat generation within the device.

In Fig. 15.6 we present threshold current densities for QD lasers (λ = 1.13 µm) of different cavity length, also from different growth runs but with identical structure. The threshold current densities are plotted versus the

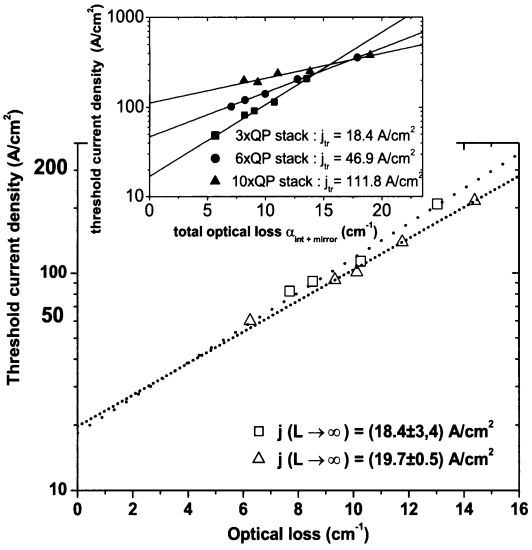

Fig. 15.6. Threshold current density versus optical loss for MOCVD-grown QD lasers, $\lambda = 1.13\,\mu$m. The different symbols (*squares* and *triangles*) depict lasers of identical structure but from different growth runs. Best values are $j_{\rm thr} = 62\ {\rm Acm}^{-2}$ (L=3.5 mm), $j_{\rm thr}(L \to \infty) < 20\,{\rm Acm}^{-2}$ (both structures), resulting in $j_{\rm thr}(L \to \infty) = 6$–$7\,{\rm Acm}^{-2}$ per QD sheet. Inset: Threshold current density versus optical loss for 3-, 6- and 10-fold QD stack lasers, $j_{\rm thr}(L \to \infty) = 18$, 47 and $112\,{\rm Acm}^{-2}$

total optical loss. In the case of a 3.5 mm long device a $j_{\rm thr} = 62\,{\rm Acm}^{-2}$ could be achieved. A transparency current density of below $20\,{\rm Acm}^{-2}$ for the triple QD stack lasers could be shown for both cases, resulting in a transparency current density of 6–$7\,{\rm Acm}^{-2}$ per single QD sheet. This is very close to the theoretically predicted value of $10\,{\rm Acm}^{-2}$ [31] and below the value of $13\,{\rm Acm}^{-2}$ of the laser reported in [34].

15.3.3 Lasing Spectra

Lateral single mode QW lasers are spectral single mode up to high output powers. Above threshold current one dominant mode emerges which suppresses other modes up to drive currents where spectral and lateral hole burning occurs. However, for some applications spectral single mode high optical power can result in spectral hole burning of the pumped medium, e.g. in fiber lasers. Therefore lateral single mode lasers with broader spectral width are sometimes needed.

In contrast to QW lasers, lateral single mode QD lasers exhibit this broader lasing spectrum as different ensembles of QDs in the active region lase independently. For a broad-area 3-fold QD laser (50 µm stripe, L=1.0 mm) the spectra for different drive currents are plotted in Fig. 15.7a. The y-scale represents the spectral power density, i.e. the area under the peak yields the total power at the given current. Lasing starts close to the maximum of the spontaneous electroluminescence (EL) and exhibits a non-Gaussian line shape. In the semi-logarithmic plot a rather broad, almost flat peak with steep sides is observed. With increasing drive current, up to 38 times the threshold current density, no saturation of the maximum intensity is observed. This fits well to theoretical calculations presented in Sect. 12.6.

The maximum width of the lasing spectra is approaching a limiting value with increasing current. In Fig. 15.7b the spectral width is plotted at a small spectral power density of 2 mW/nm. In this case the maximum spectral width is limited to about 18 nm. This width is determined by the lasing condition for the gain $g > \alpha_{\text{total}}$ (internal and mirror losses). All QDs in the center of the gain peak that fulfill this condition eventually lase; the others never overcome the losses even when completely filled with carriers. For the laser in Fig. 15.7 only about 30% of all QDs have a modal gain larger than α_{total} and contribute to the laser emission (see Fig. 15.7c). The FWHM of the EL is 46 nm and the total optical loss of 13.5 cm^{-1} (12.0 cm^{-1} mirror loss and 1.5 cm^{-1} internal loss) was derived for this laser.

In this case the influence of the first excited state of large QDs to the modal gain via the inhomogeneous broadening is neglected. These large QDs might also add to the modal gain for short cavity QD lasers that operate close to the maximum ground state gain, where a continuous shift of the lasing wavelength to the first excited state is observed with shortened cavity length.

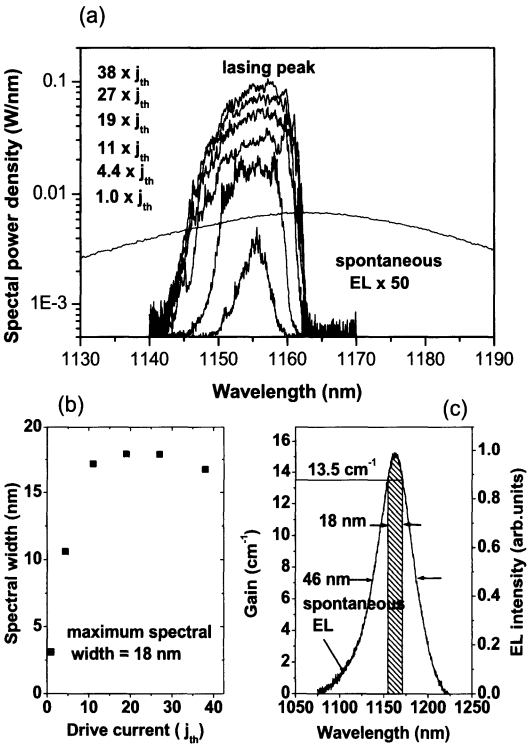

Fig. 15.7. Lasing spectra of a MOCVD-grown QD laser (50 µm stripe width, L=1.0 mm): (**a**) spontaneous electroluminescence and lasing spectra for different drive currents, (**b**) spectral width at a small spectral power density of 2 mW/nm (limiting value at high power ≈ 18 nm), and (**c**) the spontaneous, inhomogeneously broadened electroluminescence represents the size fluctuations in the QD ensemble, only the QDs in the grey area add to the lasing (within 18 nm spectral width)

15.3.4 Temperature Dependence

Since the high thermal load, generated by high output power operation, worsens the device characteristics, a good thermal stability is demanded for high power laser devices. Based on the reduced dimensionality of QDs, QD lasers were predicted to be temperature-insensitive with respect to the threshold current, making them very suitable for high power applications. However, for room temperature lasing, QD lasers have fallen far from this prediction and the realization of this key advantage remains still a challenging task.

As can be seen from the temperature dependence of the threshold current density in Fig. 15.8, this ideal QD-laser-like behavior holds only true for temperatures up to 200 K. Above this temperature the carriers escape thermally out of the QDs and are lost via (non-)radiative loss channels. The characteristic temperature T_0 is reduced from nearly infinity to typically T_0 =50–90 K.

As described in Sect. 12.5, this behavior can be modeled by incorporating the finite barrier height and decrease of quantum efficiency with temperature into the QD laser theory. As a consequence the defect-reduction in the barriers and the matrix material becomes much more crucial in QD lasers than it is already in QW lasers. Since the thermal escape rate of the carriers out of the QDs depends on the barrier height, the number of QD states and the inter-sublevel energy-spacing, various QD systems will exhibit different temperature behavior. [23,35–38]. T_0 =146 K up to 150°C for QD lasers emitting at 940 nm [23], T_0 =90 K up to 25°C for QD lasers emitting at 1.15 µm QDs [37] and T_0=250 K up to 20°C for 1.26 µm emission QD lasers [35] were reported. However, comparing T_0 values for different QD-systems is cumbersome as the QDs can be of varying quality resulting in different leakage currents that increase T_0 ostensibly. Furthermore, as pointed out in [35], the temperature dependence of the threshold current of QD lasers does not follow a strict exponential dependence, so T_0 values should only be compared for the same temperature intervals.

15.3.5 Reduced In-Plane Carrier Diffusion

As the QDs are disconnected laterally and are cladded with higher band gap material, carriers injected into the dots are confined by lateral energy barriers. Such an energy barrier should reduce the lateral diffusion of carriers from the center of the laser device toward the edges, effectively limiting the rate of lateral carrier loss. Cathodoluminescence studies on QD and QW structures demonstrate a reduced lateral diffusion resulting in an expected 50% reduction in threshold current for 1 µm-wide edge emitters or 5 µm vertical cavity surface emitting lasers (VCSELs) [9,10].

A reduced lateral carrier diffusion is not only favorable for small stripe lasers or VCSELs but also reduces the impact of defects in the active material on laser performance [11,39,40]. In Fig. 15.9 and Table 15.1 a QD and a QW laser of identical structure, except the active layer, similar lasing wavelength

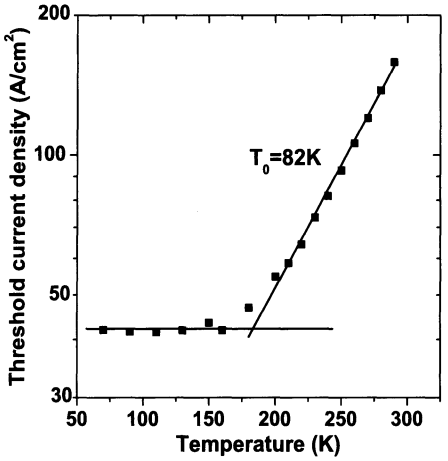

Fig. 15.8. Threshold current density versus temperature for a MOCVD-grown broad-area QD laser emitting at $\lambda = 1.16\,\mu m$ (100 µm stripe width, 1.6 mm cavity length, pulsed operation). Up to T =175 K $T_0 = \infty$ and above T_0=82 K

1160 nm / 1080 nm, threshold current densities (89 Acm^{-2}, 83 Acm^{-2}) and external quantum efficiencies (61%,68%) have been exposed to high energy proton irradiation (energy of 2.4 MeV, fluence of $2 \times 10^{13} cm^{-2}$)). Thereafter the threshold current densities 0.55 $kAcm^{-2}$ for the QD and 0.95 $kAcm^{-2}$ for the QW laser varied considerably and the external quantum efficiency was reduced to 30% and 39% respectively.

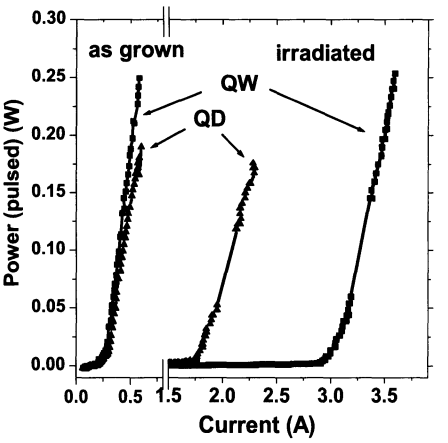

Fig. 15.9. Light-output vs. current characteristics of MOCVD-grown QD and QW laser before and after irradiation with high energy protons, for laser characteristics see table 15.1. Irradiation was performed in cooperation with N.A. Sobolev and M.C. Carmo from the University of Aveiro, Portugal

Concluding, in the spontaneous emission regime QD lasers demonstrate an enhanced radiation hardness in contrast to the QW device owing to reduced interaction of localised carriers with defects in the vicinity of the active region, leading to a comparable lower threshold. However, in the regime of lasing, both devices show similar degradation owing to barrier leakage currents leading to reduced internal efficiency. These findings indicate that the

QD approach is promising for lasers with increased lifetime, operating in a radiation environment or with an active zone in defect-rich material [11]. A possible application would be inter-satellite communication in the earths orbit where high power diode lasers with improved radiation hardness are needed.

Table 15.1. Laser device characteristics (L=1.6 mm) before and after irradiation with high energy protons (fluence: $2 \times 10^{13}\text{cm}^{-2}$, energy: 2.4 MeV)

Laser	j_{thr} (Acm^{-2})	η_{ext} (%)	Wavelength (nm)
QD, as grown	89	61	1160
QD, irradiated	550	30	1160
QW, as grown	83	68	1080
QW, irradiated	950	39	1080

15.3.6 Facet-Temperatures, COD-Levels

Today lifetime and reliability limits prevent often the widespread use of high power laser diodes in complex laser systems. Quite often the lifetime of the latter is limited by the performance of the laser diode. The catastrophic optical damage is one of the main mechanisms limiting the laser diodes lifetime. It is the result of reversible (e.g. energy-gap shrinkage) and irreversible (defect creation) microscopic processes which result in an increase of the front facet temperature due to the interplay of surface recombination, heating and increased interband reabsorption caused by energy gap shrinkage [41–44]. As 7% of the total heat power is concentrated at the front facet, facet temperatures up to 600°C have been measured for high power lasers [45].

The reduced carrier diffusion in QD layers as compared to the one in QWs should reduce the transport of carriers to the facet. Therefore one expects reduced front facet heating for QD lasers. By the means of micro-Raman spectroscopy the brightest spot of the front facet area can be singled out and the temperature increase over injection current can be monitored. As the probing depth is about 200 nm the true front facet temperature is measured. The increase in bulk temperature is deduced by the shift of the lasing wavelength. In Fig. 15.10 with the means of micro-Raman spectroscopy the temperature of the front facet is investigated for a QD and a QW laser of identical structure, except the active layer, quantum efficiency ($\eta_{\text{ext}} = 82\%$ / $\eta_{\text{ext}} = 74\%$), threshold current ($j_{\text{thr}} = 114\,\text{Acm}^{-2}$ / $j_{\text{thr}} = 101\,\text{Acm}^{-2}$) and wavelength ($\lambda = 1150\,\text{nm}$ / $1080\,\text{nm}$).

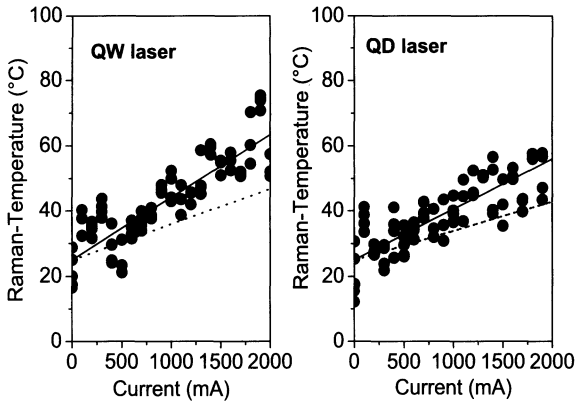

Fig. 15.10. Front facet temperature (pulsed mode) for a QD and a QW laser by the means of Raman spectroscopy, performed at the Max-Born-Institute, Berlin, Germany

In a previous experiment of a MBE-grown QD laser at 940 nm with facet coatings and in cw operation no increased heating of the facet area as compared to the bulk-temperature could be detected. In this present experiment as cleaved facets and pulsed mode was used. Up to a current of 2.0 A the temperature increase for the facet of the QD laser is smaller than for the QW laser. Unfortunately the pulse generator to drive the diode lasers is limited to 2.0 A, so the superiority of the QD laser could not be made more clear in this experiment.

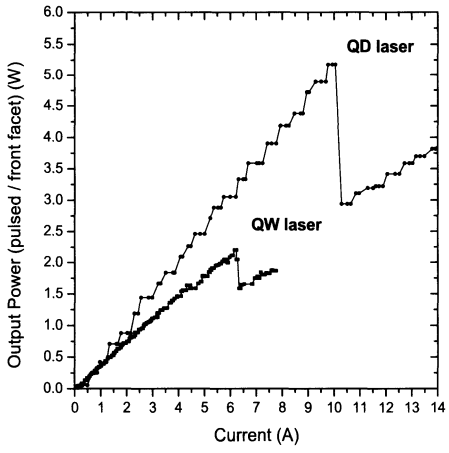

Fig. 15.11. Light-output vs. current characteristics up to degradation for a 6-fold QD and a single-QW laser (stripe width 100 µm, cavity length L=1.6 mm, HR/AR coating, pulsed operation, f=1 kHz, P_{width}=0.5 µs). The device characteristics were: QW: λ =1.08 µm, slope=0.39 W/A, j_{thr}=71 Acm^{-2}, P_{max}=2.2 W, COD-level=5.5 MWcm^{-2} and QD: λ =1.16 µm, slope=0.55 W/A, j_{thr}=131 Acm^{-2}, P_{max} =5.2 W, COD-level=13 MWcm^{-2}

For a different set of broad-area (100 µm stripe width) single QW and 6-fold QD lasers with HR/AR facet coatings the light output characteristic in pulsed mode is taken up to degradation (Fig. 15.11). Except for the active region, the structure of the two lasers is identical. The QW laser exhibits a front facet output power of 2.2 W at a COD-level of 5.5 MW/cm^2, the QD laser 5.2 W output power and 13 MW/cm^2 COD-level, respectively. As the

pulse-width is only 500 ns and the repetition rate f=1 kHz, heating effects on the COD-level should be negligible.

15.4 Summary

Today, QD lasers surpass QW lasers already in many respects. This has been achieved by considerable improvements in the quantum dot heterostructure growth and the advantage that the QDs as active material can be easily combined with standard high-power diode laser technology. We have shown how the introduction of an annealing step in the growth process can reduce defects in the matrix material and improve laser device performance. High power operation accompanied with low threshold current densities and high quantum efficiencies could be demonstrated. Due to the reduction of the number of states, QD lasers show today the lowest threshold current densities for any diode laser. In contrast to single mode QW lasers which are spectral monomode, QD lasers will always show spectral multi-mode behavior. This broad lasing spectra however might be favorable for certain pump-applications.

It turned out to be a more challenging task to realize the promised temperature insensitivity of QD laser device characteristics. The 1.3 µm QD lasers with a T_0 =250 K already surpasses standard InP-based telecommunication QW lasers by far, typical T_0 is about 50 K. However, to improve the temperature characteristics of 940 nm or 1100 nm QD lasers probably new approaches and ideas will be needed.

The reduced in-plane carrier diffusion due to the localization of carriers in the QDs improves threshold currents for small stripe lasers as well as for VCSELs. Furthermore, QD lasers demonstrate enhanced radiation hardness to high energy irradiation as compared to QW lasers owing to the reduced interaction of the carriers with defects in the vicinity of the QDs. Finally, QD lasers show reduced facet heating under high power operation resulting in higher COD levels, allowing for higher optical output powers and longer lifetimes than comparable QW lasers. Thus for high power laser diodes the QD approach turned out to be very fruitful and will probably substitute QW technology in the long run.

Acknowledgment

We like to thank Prof. N.N. Ledentsov for providing the results of the 940 nm QD lasers shown in Fig. 15.4, Dr. P. Werner and Dr. N. Zakharov from the Max-Planck-Institut für Mikrostrukturphysik in Halle for the TEM-images of Fig. 15.3, Dr. J.W. Tomm at the Max-Born-Institut in Berlin for performing the micro-Raman measurements on the laser front facets shown in Fig. 15.9 and Prof. N.A. Sobolev and Dr. M.C. Carmo from the University of Aveiro, Portugal, for the high energy proton irradiation of our QD and QW lasers shown in Fig. 15.9. For further support and fruitful discussions we thank

Dr. V.M. Ustinov and D.A. Livshits form the Ioffe-Institute in St. Petersburg, Russia and Dr. G. Erbert, Dr. R. Hülsewede, Dr. W. Pittroff, Dr. R. Staske and Dr. H. Wenzel from the Ferdinand-Braun-Institut, Berlin.

References

1. *High-Power Diode Lasers, Fundamentals, Technology, Applicatons*, ed. by R. Diehl (Springer, Heidelberg 2000)
2. S. O'Brien, H. Zhao, A. Schoenfelder, R.J. Lang: Electron. Lett. **33**, 1869 (1997)
3. S. O'Brian, A. Schoenfelder, R.J. Lang: IEEE Photon. Technol. Lett. **9**, 1217 (1997)
4. D.A. Livshits, I.V. Kochnev, V.M. Lantrov, N.N. Ledentsov, R.A. Nalyot, I.S. Tarasov, Zh.I. Alferov: Electron. Lett. **36**, 1848 (2000)
5. H.G. Treusch, J. Harrison, B. Morris, J. Powers, D. Brown, J. Martin: Proc. SPIE **3945**, 23 (2000)
6. E.B. Mejia, A.N. Starodumov, Yu.O. Barmenkov: Appl. Phys. Lett. **74**, 1540 (1999)
7. H. Wenzel, G. Erbert, F. Bugge, A. Knauer, J. Maege, J. Sebastain, R. Staske, K. Vogel, G. Tränkle: Proc. SPIE **3947**, 32 (2000)
8. Y. Arakawa, H. Sakaki: Appl. Phys. Lett. **40**, 939 (1982)
9. J.K. Kim, T.A. Strand, R.L. Naone, L.A. Coldren: Appl. Phys. Lett. **74**, 2752 (1999)
10. J.K. Kim, R.L. Naone, L.A. Coldren: IEEE J. of Quantum Electron. **QE-6**, 504 (2000)
11. C. Ribbat, R. Sellin, M. Grundmann, D. Bimberg, N.A. Sobolev, M.C. Carmo: Electron. Lett. **37**, 174 (2001)
12. T.C. Newell, D.J. Bossert, A. Stintz, B. Fuchs, K.J. Malloy, L.F. Lester: IEEE Photon. Technol. Lett. **11**, 1527 (1999)
13. J.R. Marciante, P. Agrawal: IEEE J. of Quantum Electron. **QE-32**, 590 (1996)
14. J.R. Marciante, P. Agrawal: IEEE J. of Quantum Electron. **QE-33**, 1174 (1997)
15. M.V. Maximov, A.F. Tsatsulnikov, B.V. Volovik, D.S. Sizov, Yu.M. Shernyakov, I.N. Kaiander, A.E. Zhukov, A.R. Kovsh, S.S. Mikhrin, V.M. Ustinov, Zh.I. Alferov, R. Heitz, V.A. Shchukin, N.N. Ledentsov, D. Bimberg, Yu.G. Musikhin, W. Neumann: Phys. Rev. B **62**, 16671 (2000)
16. M.M. Sobolev, I.V. Kochnev, V.M. Lantratov, N.A. Bert, N.A. Cherkashin, N.N. Ledentsov, D.A. Bedarev: Semiconductors **34**, 195 (2000)
17. R.L. Sellin, Ch. Ribbat, M. Grundmann, N.N. Ledentsov, D. Bimberg: Appl. Phys. Lett. **78**,1207 (2001)
18. R.L. Sellin, F. Heinrichsdorff, Ch. Ribbat, M. Grundmann, U.W. Pohl, D. Bimberg: J. Cryst. Growth **221**, 581 (2000)
19. F. Heinrichsdorff, Ch. Ribbat, M. Grundmann, D. Bimberg: Appl. Phys. Lett. **76**, 556 (2000)
20. M. Grundmann, F. Heinrichsdorff, C. Ribbat, M.-H. Mao, D. Bimberg: Appl. Phys. B **69**, 413 (1999)
21. B. Bockelmann, G. Bastard: Phys. Rev. B **42**, 8947 (1990)
22. H. Benisty, C.M. Sotomayor-Torres, C. Weisbuch: Phys. Rev. B **44**, 10945 (1991)
23. F. Schäfer, J.P. Reithmaier, A. Forchel: Appl. Phys. Lett. **74**, 2915 (1999)

24. V.M. Maximov, I.V. Kochnev, Y.M. Shermyankov, S.V. Zaitsev, N.Yu. Gordev, A.F. Tsatsul'nikov, A.V. Sakharov, I.L. Krestnikov, P.S. Kop'ev, Zh.I. Alferov, N.N. Ledentsov, D. Bimberg, A.O. Kosogov, P. Werner, U. Gösele: J. Appl. Phys. **83**, 5561 (1998)
25. Ch. Ribbat, R. Sellin, M. Grundmann, D. Bimberg: phys. stat. sol. (b) **3**, 819 (2001)
26. A.R. Kovsh, A.E. Zhukov, D.A. Livshits, A.Yu. Egorov, V.M. Ustinov, M.V. Maximov, Yu.G. Musikhin, N.N. Ledentsov, P.S. Kop'ev, Zh.I. Alferov, D. Bimberg: Electron. Lett. **35**, 1161 (1999)
27. F. Klopf, J.P. Reithmaier, A. Forchel: Appl. Phys. Lett. **77**, 1419 (2000)
28. F. Klopf, J.P. Reithmaier, A. Forchel, P. Collot, M. Krakowski, M. Calligaro: Electron. Lett. **37**, 353 (2001)
29. R. Heitz, H. Born, T. Lüttgert, A. Hoffmann, D. Bimberg: phys. stat. sol. (b) **221**, 65 (2000)
30. A.E. Zhukov, A.R. Kovsh, S.S. Mikhrin, N.A. Maleev, V.M. Ustinov, D.A. Livshits, I.S. Tarasov, D.A. Bedarev, M.V. Maximov, A.F. Tsatsulnikov, I.P. Soshnikov, P.S. Kop'ev, Zh.I. Alferov, N.N. Ledentsov, D. Bimberg: Electron. Lett. **35**, 1845 (1999)
31. M. Grundmann, D. Bimberg: Jpn. J. Appl. Phys. **36**, 4181 (1997)
32. G. Park, O.B. Shchekin, D.L. Huffaker, Q. Mo, D.G. Deppe: IEEE Photon. Technol. Lett. **12**, 1120 (2000)
33. G.T. Liu, A. Stintz, H. Li, T.C. Newell, A.L. Gray, P.M. Varangis, K.J. Malloy, L.F. Lester: IEEE J. of Quantum Electron. **QE-36**, 1272 (2000)
34. P.G. Eliseev, G.T. Liu, A. Stintz, H. Li, T.C. Newell, K.J. Malloy, L.F. Lester: Appl. Phys. Lett. **77**, 262 (2000)
35. G. Park, O.B. Shchekin, D.L. Huffaker, D.G. Deppe: Appl. Phys. Lett. **77**, 466 (2000)
36. Yu.M. Shernyankov, D.A. Bedarev, E.Yu. Kondrateva, P.S. Kopev, A.R. Kovsh, N.A. Maleev, V.M. Maximov, S.S. Mikhrin, A.F. Tsatsulnikov, V.M. Ustinov, B.V. Volovik, A.E. Zhukov, Zh.I. Alferov, N.N. Ledentsov, D. Bimberg: Electron. Lett. **35**, 898 (1999)
37. M. Sugawara, K. Mukai, Y. Nakata: Appl. Phys. Lett. **76**, 3349 (2000)
38. K. Mukai, Y. Nakata, K. Otsubo, M. Sugawara, N. Yokoyama, H. Ishikawa: Appl. Phys. Lett. **76**, 3349 (2000)
39. R. Leon, G.M. Swift, B. Magness, W.A. Taylor, Y.S. Tang, K.L. Wang, P. Dowd, Y.H. Zhang: Appl. Phys. Lett. **76**, 2074 (2000)
40. P.G. Piva, R.D. Goldberg, I.V. Mitchell, D. Labrie, R. Leon, S. Charbonneau, Z.R. Wasilewski, S. Farfard: Appl. Phys. Lett. **77**, 624 (2000)
41. M. Fukuda: *Reliability and Degradation of Semiconductor Lasers and LEDs* (Artech House, Boston, London 1991)
42. G. Chen, M. Okayasu, J. Temmyo: J. Appl. Phys. **74**, 2167 (1993)
43. M. Fukuda, M. Okayasu, J. Temmyo, J. Nakano: IEEE J. of Quantum. Electron. **QE-30**, 471 (1994)
44. C.H. Henry, P.M. Petroff, R.A. Logan, F.R. Merrit: J. Appl. Phys. **50**, 3721 (1979)
45. R. Puchert, J.W. Tomm, A. Jaeger, A. Bärwolff, J. Luft, W. Späth: Appl. Phys. A **66**, 483 (1998)